THE ROLE OF MICROSTRUCTURE AND NOTCH ROOT RADIUS ON THE FRACTURE TOUGHNESS OF A MARTENSITE STRUCTURE STEEL

D.Firrao°, R.Roberti°°, G.Silva°°

The fracture toughness of as quenched AISI 4340 steel was studied as a function of notch root radius, inclusion content and austenitic grain size. An aircraft quality sulfide containing steel (A), a commercial quality heat with oxides and sulfides (B) and a VAR 4340 steel (C) were investigated. In all the cases, the sharp crack fracture toughness was improved by a 1200-870°C step-quench heat treatment, compared to a conventional 870°C austenitize-quench procedure; instead, the blunt notch fracture toughness of the conventionally austenitized specimens resulted consistently higher than that of the ones austenitized at high temperature. The comparison between the steels was made by means of plots of the applied J at fracture vs. notch root radius.

INTRODUCTION

A recent series of studies (1,2,3) has clarified the fracture mechanisms governing fracture initiation and propagation at the root of stress concentrations of various severity in as-quenched AISI 4340 notched bend specimens. In such a metallurgical condition this steel is characterized by a very low strain hardening coefficient; it can thus be considered as representative of all the metal alloys prone to flow localization and therefore to the activation of plastic instabilities along slip lines when loaded to fracture(4).

In specimens austenitized one hour at 870 to 1200°C the following sequence of events was seen to occur at a blunt notch under increasing loads:

(i) multiple crack nucleation along the root of the stress concentration as a consequence of high tensile stress in a thin surface layer damaged by machining. These microcracks extend in radial directions to a depth of 20-22 μm, independently of notch root radius and austenitic grain size;

(ii) further propagation of fracture along logarithmic spiral directions pertaining to the slip line field existing below the stress free cylindrical annulus created by the multiple crack formation (Fig.1a). Rupture surfaces in this stage depart from position close to either of two microcracks almost symmetrically displaced from the notch center plane in the direction normal to it and propagate towards the notch midsection (Fig.1b);

(iii) final crack propagation through the specimen minimum cross section.

Step (ii) is characteristic of the specimens with small grain size. In specimens austenitized at 1200°C fracture along logarithmic slip directions appeared only in a few zones at the stress concentration, when the notch root radius, ρ, passed a limiting value (ρ_{eff}) of the same order of the austenitic crystal average dimensions (250 μm). Also in the sharp notched specimens quen-

° Dipartimento di Scienza dei Materiali e di Ingegneria Chimica, Politecnico di Torino
°° Dipartimento di Chimica-Fisica Applicata, Politecnico di Milano

ched from 870°C with ρ smaller than ρ_{eff} (also here of the same order of the austenitic grain size, 20 μm) step (ii) was not seen in the fracture path; rupture initiated and propagated in a region close to the notch center-plane.

It is now intended to assess the influence of the inclusion content and distribution, and of the prior austenitic grain size on the above illustrated sequence of events as well as on the blunt notch fracture toughness of as-quenched AISI 4340 steel. An aircraft commercial quality heat (hereafter indicated as steel B) and a Vacuum Arc Remelted one (steel C) have been selected to compare their behaviour with that of the aircraft quality heat already examined (steel A, ref. 1,2). Furthermore the austenitizing procedures have been designed to obtain three different ranges of grain sizes, namely, 18-20, 75-85, and 215-250 μm in order to determine the role of the grain size among the factors proposed to control the toughness of as-quenched AISI 4340 in the case of sharp cracks or blunt notches , object of debate in the recent literature (2,6,7,8).

MATERIALS AND EXPERIMENTAL PROCEDURE

Charpy-V type specimens with notch root radii from fatigue precrack up to 1.6 mm were fabricated with standard thickness of 10 mm. The chemical analysis of the AISI 4340 steels compared in the present study is given in Table I. Both steel A and B were produced in an electric arc furnace, whereas steel C was fabricated by Vacuum Arc Remelting (VAR). All the steels were received in the hot rolled and annealed condition. Steel A was in the form of a 50mm square bar (5), steel B and C as 70 and 85 mm dia. cylindrical bars. Notches and fatigue precracks were machined in the LT direction for steel A (5), and in the LR direction for steel B and C. The axes of the tensile specimens were all in the longitudinal direction.

Three different austenitize-quench cycles were adopted for the heat-treatments performed after machining steel B and C samples. These were conventional treatment to 870°C for 1 h followed by an oil quench and austenitize for 1 h at 1200°C with subsequent cooling to 870°C for one-half hour prior to the oil quench. This step quench (hereafter referred to as 1200-870°C treatment) was the same as adopted in the previous studies on steel A (1,2,5) for the ease of comparison of results. A few samples with ρ > 0.25 mm were heat-treated keeping them only 40 min. at 1200°C prior to the step-quench in order to limit grain growth. The whole heat-treating procedure was performed in salt baths carefully controlled for neutrality.

Non metallic inclusions were observed by means of a Baush & Lomb, Omnicon Alpha image analyser on transverse sections and on the longitudinal surfaces by an ETEC Co. Omniscan model Scanning Electron Microscope coupled to a Tracor Northern, TN 2000, Energy Dispersion Spectrometer. The same SEM was employed for fractography.

A 100 kN floor model INSTRON 1195 machine was used for the mechanical tests; they were performed at a crosshead speed of 0.0083 m/s. Test fixture span for the three point bend specimens was 40 mm. Since the load-deflection diagrams were essentially linear up to instability and subcritical crack growths almost nil, as in the case of steel A, K values calculated at maximum load were employed to obtain critical applied J-integral values by the relationship $J = (1 - \nu^2) \cdot K^2/E$.

TABLE I - Chemical composition of the AISI 4340 steels (wt.pct.)

	C	Ni	Cr	Mo	Mn	Si	P	S
Steel A	0.40	1.74	0.81	0.23	0.75	0.26	0.019	0.015
Steel B	0.41	1.69	0.78	0.24	0.75	0.27	0.016	0.015
Steel C	0.41	1.80	0.85	0.26	0.82	0.22	0.009	0.003

TABLE II - Microstructural characteristics of steels

Steel	$d_{g.s.}$ (μm)	d (μm)	f (%)	D_s (μm)	λ (μm)
A	20° 250°°	10.2	$2.6 \cdot 10^{-2}$	50	256
B	20° 82°°° 215°°	7.2	$2.4 \cdot 10^{-2}$	37	194
C	20° 78°°° 200°°	7.8	$8.5 \cdot 10^{-3}$	68	606

°1 h at 870°C; °°1 h at 1200°C; °°°40 min. at 1200°C

RESULTS

Microstructural Analysis

The microstructural characteristics of the steels are listed in Table II. Although steels A and B have very similar composition, the inclusion type and distribution were quite different; in steel A it was possible to recognize only elongated sulfides, whereas in steel B thin sulfides were accompanied by a few larger round inclusions, identified as silicon-aluminates. Steel C had a very limited amount of slightly elongated sulfides and widely spaced round inclusions.

Mechanical Tests

Standard room temperature tensile properties of the three types of AISI 4340 steels are reported in Table III. High temperature austenitizing resulted in lower values of the ultimate tensile strength and in a negligible (steels A and B) or a small variation (steel C) of the yield strength.

J-integral values applied at maximum load versus notch root radius appear in Fig. 2 for steels B and C along with the dotted lines interpolating results pertaining to steel A. The close resemblance of plots pertaining to steels B and C with those obtained averaging steel A data is evident. The occurrence of a limiting root radius (ρ_{eff}) below which fracture toughness stays constant is clearly established either for coarse or fine grained structures. Furthermore for ρ values greater than ρ_{eff} the existence of sloped lines extrapolating to the origin is confirmed either in the case of conventionally austenitized specimens or with the step-quenched ones. The latter finding is particularly important since the interpretation of steel A results in this range of ρ's was partially dubious. After a second limiting value of ρ, which varied with the steel and heat treat-

TABLE III - Tensile properties of the steels in the as-quenched condition

Steel	Austenitizing Treatment	0.2 pct Proof Stress (MPa)	Ultimate Tensile Strength (MPa)	Elongation to fracture (%)
A	870°C	1695	2060	5.2
A	1200-870°C	1715	1980	3.2
B	870°C	1710	2108	7.5
B	1200-870°C	1705	1930	4.2
C	870°C	1818	2233	6.8
C	1200-870°C	1738	1965	3.0

ment, less sloped lines take place in the field of large root radii.

Fractographic Observations

Fracture of precracked specimens and of all the blunt notch ones with $\rho < \rho_{eff}$ was of the brittle intergranular type for all the steels and heat treatments over the whole fracture surface.

In the case of conventionally austenitized samples with $\rho > \rho_{eff}$ shear lips formed along the notch root at all points except for a small central portion (Fig.3.1) where integranular brittle fracture predominated either at the notch (Fig.3.2) or just behind (Fig.3.3). Multiple microcrack formation was seen at the notch root as in the case of steel A (1), so that characteristic shear dimples were evident only beginning 25 μm ca. from the root surface (Fig.3.2'). The fracture after the propagation along logarithmic spirals was mainly of the ductile trangranular type, with a few areas of quasi-cleavage (Fig.3.3'). On most of the surface of the microcracks formed at the notch root fine dimples covered integranular facets (Fig. 4a) with transgranular cleavage (Fig.3.2') occurring only at a few locations close to the specimen center. Shear lip fracture morphologies differed considerably in steel B and C samples. With the former steel, rupture surfaces were predominantly flat with relatively large elongated dimples dotting it, whereas in the case of the latter very fine dimples covered the whole slip area (Fig.5).

All the specimens step-quenched from 1200°C with $\rho > 0$ again exibited a multiple microcrack formation at the notch root with a dimpled fracture morphology (Fig.4b). Steel B and C samples with the intermediate grain size (80μm ca.) characterized by values of ρ greater than 0.5 mm ca. also showed almost continuous shear lip of rather limited extension emanating from the above mentioned stress free annulus. Such a feature had been seen only at very few locations in steel A samples which had a very coarse grained structure. After propagation along slip directions the fracture resumed again a prevalently intergranular morphology as in the case of smaller root radius specimens. Some amount of ductile tearing was evident on the intergranular facets in samples with the largest root radii.

Optical microscopy measurements of the longitudinal projection of the slip portion of the fracture surface were performed on the samples which exibited an almost continous shear lip formation at the root of the notch. Results of observations at multiple locations along the thickness have been averaged and the procedure already detailed in Ref.1 has been followed to obtain the values of the β' angles pertaining to the slip surfaces along which fracture propagated from the stress free zone determined by the above described multiple microcracks (Fig.1a). The variation of such an angle with the root radius is illustrated by Fig.6a for conventionally quenched samples and by Fig.6b for the high temperature austenitized ones. Fig.6a again confirms that β' stays constant at a high level when ρ is small and then starts to decrease in correspondance of the ρ values at which the $J-\rho$ line passing through the origin in Fig.2 is no longer followed. Moreover, whereas results pertaining to steel B testpieces are close to those of steel A samples, β' values for steel C start from a higher level before falling down to eventually enter a unique scatterband encompassing all the data pertaining to large ρ specimens. Experimental points in Fig.6b instead show that in high temperature austenitized samples, when fracture propagated along slip lines, it departed from the notch at an almost constant low angle, whichever the root radius or the cleanness of the steel.

INTERRELATION BETWEEN MICROSTRUCTURE AND FRACTURE TOUGHNESS

Sharp Crack Samples

K_{Ic} values are compared in the following Table IV along with ρ_{eff} values

TABLE IV - K_{Ic} values for as-quenched AISI 4340 steel

Steel	ρ_{eff} (mm)	$d_{g.s.}$ (μm)	K_{Ic} ($MN/m^{3/2}$)	Steel	ρ_{eff} (mm)	$d_{g.s.}$ (μm)	K_{Ic} ($MN/m^{3/2}$)
A	0.015	20	43.1	A	0.230	250	73.9
B	0.034	34	43.1	B	0.144	215	54.4
C	0.025	18	42.1	C	0.098	200	47.5

and austenitic grain sizes.

With fine austenitic grain sizes it is evident that the Vacuum Arc Remelting procedure does not cause any improvement in the plane strain fracture toughness. Such a mechanical characteristic then is not influenced by the inclusion content in the case of brittle integranular fracture. The same holds upon examining the results of coarse grained steels. In such a case, Table IV data would even signal that the cleaner the steel, the less the fracture toughness improvement imparted by high temperature austenitizing. It is than obvious that some other parameter influences the fracture toughness of coarse grained structures.

A model to link sharp cracked samples data with blunt notch specimens results has been proposed by Ritchie and coworkers (6,7) incorporating previous derivations by Tetelman et al. (9,10). The proposed mathematical relationship which is valid for stress controlled fractures reads,

$$K_{Ic} \simeq 2.9 \ \sigma_Y \left[\exp \left(\sigma_f / \sigma_Y - 1 \right) - 1 \right]^{1/2} \cdot \rho_{eff}^{1/2} \qquad (1)$$

where σ_Y is the yield stress and σ_f the critical fracture stress. Since $K_{Ic}/\sqrt{\rho_{eff}}$ does not vary appreciably, as proved in the subsequent section, the fracture toughness should directly relate to $\sqrt{\rho_{eff}}$. This is verified by present results, since, K_{Ic}'s for steels A, B and C are in the sequence of ratios 1.55, 1.15 and 1, whereas $\sqrt{\rho_{eff}}$ varies as 1.53, 1.21 and 1.

The possibility to substitute $d_{g.s.}$ for ρ_{eff} into Eq.1 is only partially proved. Both these quantities decrease passing from steel A to steels B and C, but there is not a one to one correspondance between them.

A comparison of results pertaining to specimens quenched from 870°C with those of step-quenched samples on the basis of Eq.1 is not possible, since present blunt notch data do not allow to obtain any information about σ_f for fine grained structures (see below). It can only be stated that in this case to a constancy of ρ_{eff} and $d_{g.s.}$ for the three steels corresponds a constancy of K_{Ic}.

From the above considerations it can thus be concluded that the austenitic grain size is the microstructural parameter that plays the most significant role in controlling the fracture toughness when brittle intergranular fractures occur. A mathematical relationship between K_{Ic} and $d_{g.s.}$ valid in all cases is not available, although Eq.1 can be of use in some cases putting $d_{g.s.}$ in place of ρ_{eff}.

Blunt Notch Samples

As already pointed out before (2) fracture propagation through slip surfaces strongly influences toughness results. Furthermore, since such a rupture is of the ductile type, Eq.1 with ρ in place of ρ_{eff} and K replacing K_{Ic} cannot be applied to interpret results when shear lips are present on the fracture surface. Its use is therefore restricted to a few data pertaining to coarse grained samples with $\rho_{eff} < \rho < 0.5$ mm ca., where fracture nucleation was seen to be intergranular. In this range the interpolating lines are almost coincident thus signaling that $dK/d\sqrt{\rho}$ is the same for all the steels.

Shear lips are present in all the blunt notch specimens quenched from

870°C with $\rho > \rho_{eff}$. In Fig.7 J values applied at fracture have been plotted as a function of s', the arc of slip line travelled by the crack before final propagation through the specimen minimum cross section. It is conspicuous that straight lines are obtained also with steel B and C specimens as it was evident with steel A samples (2). Furthermore, in correspondance with J - ρ plots being almost coincident for steels A and B, J - s' plots for these steels superimpose. Steel C which displayed higher fracture toughness than steels A and B at corresponding values of ρ, is characterized by much higher J-integral values applied at fracture than steels A and B at equal s' lengths. This is confirmed by the fracture morphologies of the slip surfaces which also indicated (Fig.5) that a more intense resistance is offered to slip by steel C samples. The mechanical test results lead to the further conclusion that the maximum strain that can be sustained at the notch root before fracture ($\varepsilon_{max,f}$) is strongly influenced by the inclusion volume fraction. In fact, a model has been recently developed by Firrao and Roberti (12) to relate J-integral values applied at fracture initiation of notched specimens (J_A) to ρ and $\varepsilon_{max,f}$. Their formulation reads,

$$J_A = \sigma_Y^{(1-N)} \cdot \varepsilon_{max,f}^{(1+N)} \cdot E^N \cdot \rho / F(\Gamma(N)) \qquad (2)$$

where $F(\Gamma(N))$ is a mathematical function of the strain hardening exponent N. The relationship is valid only when J - ρ plots pass through the origin. N has been determined as 0.03 ca. for all the steels. Therefore a direct correspondance between J/ρ and $\varepsilon_{max,f}$ arises from Eq.2. Since steels A and B, which contain an almost equal volume fraction of inclusions, yield equal J/ρ values, they are characterized by the same value of $\varepsilon_{max,f}$. To steel C, which displays a lower inclusion content and a higher slope in the J - ρ plot, a larger limiting strain at the notch root is associated.

A final analysis has to be performed about the factors that favour the occurrence of shear lip fractures instead of the intergranular ones. Data obtained with intermediate grain size (80 μm ca.) samples, step-quenched from 1200°C, seem to indicate that small garin sizes allow an easier establishment of active slip systems at the root of a notch. A rationale can then be developed on such a basis. When ρ increases the plastic zone at the root of the concentration enlarges up to the point that it comprises a few grains. Only then macroscopic plastic instabilities along slip directions can be activated.

CONCLUSIONS

It has been proved that the austenitic grain size is directly related to the fracture toughness (K_{Ic}) of AISI 4340 steel, which fractures by an intergranular process. In such a case the cleanness of the steel has no evident influence on K_{Ic}. In the case of blunt notch specimens, the smaller the grain size the easier is the possibility of ductile shear slip ruptures at the root of the notch. When these fractographic features are present applied J-integral values at failure are linearly related to their size and increase as the volume fraction of the inclusions decreases.

SYMBOLS USED

ρ = notch root radius in a Charpy-V type specimen

$\varepsilon_{max,f}$ = maximum strain at fracture nucleation at the root of a stress concentration

$d_{g.s.}$ = austenitic grain size

d = average diameter of inclusions (transverse surface)

f = inclusion volume fraction

D_s = average center to center spacing of inclusions

λ = average mean free path of inclusions

Work partially supported by CNR (CTB 80-0108801)

REFERENCES

1. Firrao,D.,Begley,J.A.,DeBenedetti,B.,Roberti,R.,and Silva,G.,1980,Scripta Met.,14,519

2 Firrao,D.,Begley,J.A.,Roberti,R.,Silva,G.,and DeBenedetti,B.,1982,Metall. Trans.A,13A,1003

3 Firrao, D., and Roberti,R.,1981,Metall.Ital.,73,337

4 Spretnak,J.W., and Firrao,D.,1980,Metall.Ital.,72,525

5 Roberti,R.,Silva,G.,DeBenedetti,B., and Firrao,D.,1978,Metall.Ital.,70,449

6 Ritchie,R.O.,Francis,B., and Server,W.L.,1976,Metall.Trans.A,7A,831

7 Ritchie,R.O., and Horn,R.M.,1978,Metall.Trans.A,9A,331

8 Khan,K.H., and Wood,W.E.,1978,Metall.Trans.A,9A,899

9 Wilshaw,T.R.,Rau,C.A., and Tetelman,A.S.,1968,Eng.Fract.Mech.,1,191

10 Malkin,J., and Tetelman,A.S.,1971,Eng.Fract.Mech.,3,151

11 Firrao,D., and Roberti,R.,1982,"Convegno Chimica dello Stato Metallico", Levrotto & Bella, Torino, Italia,223

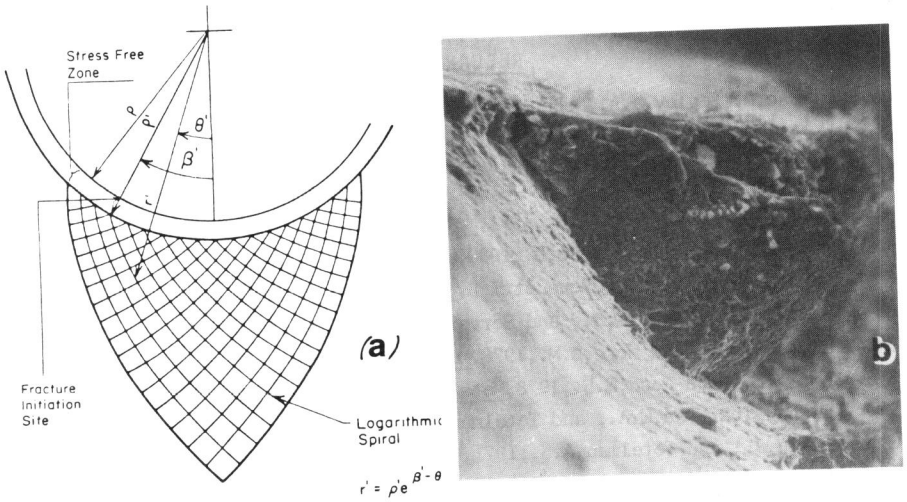

Figure 1 Modified slip line field at a notch (a), where fracture propagates along logarithmic spirals (b)

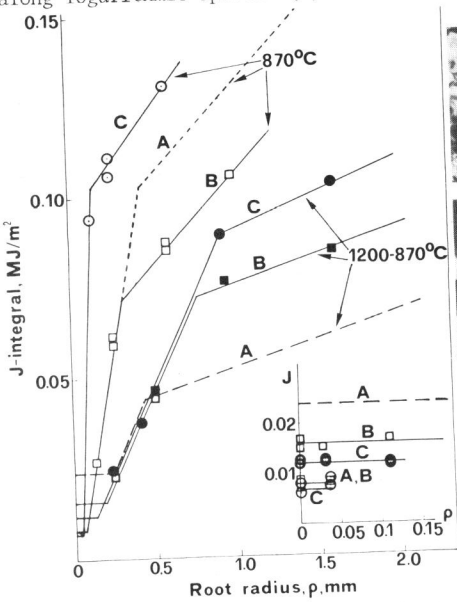

Figure 2 J-int. at failure vs. root radius (●■ samples held 40 min. at 1200°C)

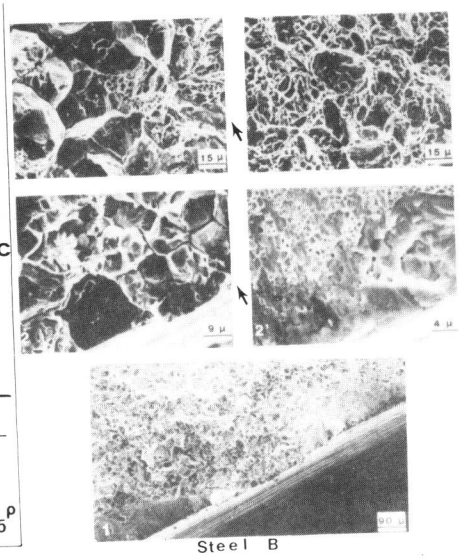

Figure 3 Fracture morphologies for a sample quenched from 870°C (ρ=0.6 mm)

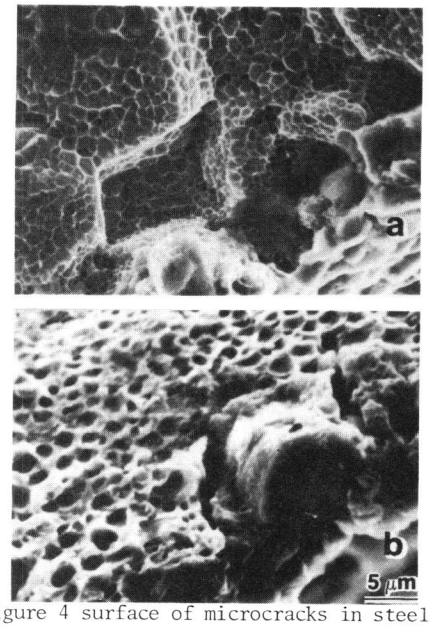

Figure 4 surface of microcracks in steel C samples quenched from 870 (a) or 1200°C (b)

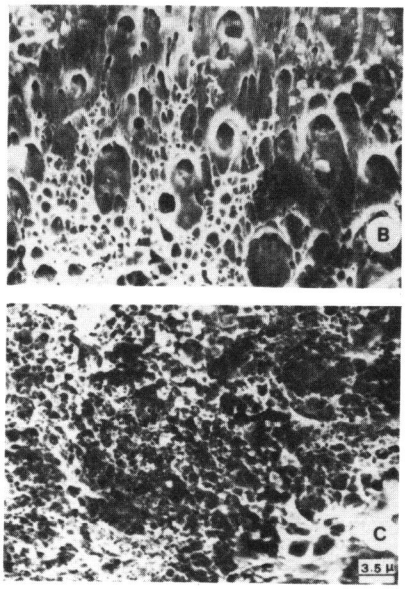

Figure 5 Shear slip surfaces in steel B and C samples quenched from 870°C

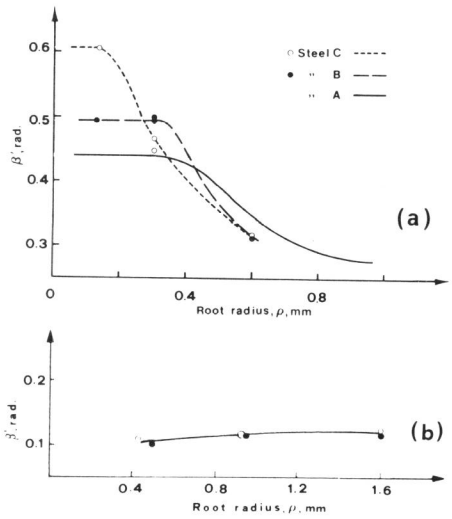

Figure 6 Values of β' angles in samples quenched from 870 (a) or 1200°C (b)

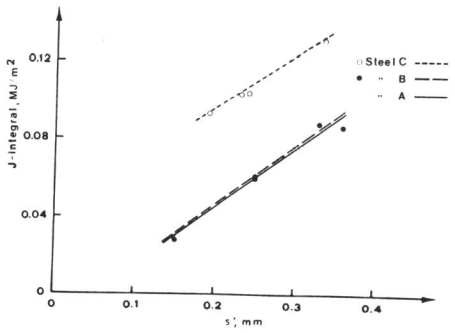

Figure 7 J-int. vs. length, s', of the arc of slip lines travelled by the crack